Bulletin of Earthquake Engineering (2023) 21:1685–1711
https://doi.org/10.1007/s10518-022-01381-4

S.I.: ADVANCES ON INERTER-BASED SEISMIC PROTECTION OF STRUCTURES

Design of MDOF structure with damping enhanced inerter systems

Ruifu Zhang[1,2] · Minjun Wu[1,2] · Chao Pan[3] · Chao Wang[1,2] · Linfei Hao[4]

Received: 3 August 2021 / Accepted: 6 March 2022 / Published online: 6 April 2022

Abstract

An inerter is a two-terminal inertial element that can produce an amplified inertance and enhanced damping when operating with spring and damping elements. Its superior vibration mitigation effect has been proved by previous studies. Although H∞ optimal design of inerter-controlled single-degree-of-freedom structure can be derived based on fixed-point method, rational and theoretical design methods for inerter-controlled multi-degree-of-freedom (MDOF) structures yet need to be developed. In this study, a practical and semi-analytical method based on the damping enhancement principle is proposed for the design of inerter-controlled MDOF structures under earthquakes. To improve the vibration mitigation efficiency, the parameters of inerter systems are distributed based on structural responses, and the required damping coefficient in the inerter systems is minimized to fully utilize the damping enhancement effect of inerter systems. The response mitigation ratio is taken as the targeted performance index to fulfill the demand-oriented design philosophy presented in this study. The stochastic response of the structure is obtained by conducting complex mode superposition. A detailed design procedure and corresponding computer program is developed. Three benchmark structures are employed to exemplify the effectiveness of the proposed design. The analysis results show that the story drifts and story shear forces of the designed structure are effectively mitigated to the target value. In comparison with an existing method (the fixed-point method), the proposed design strategy efficiently exploits the damping enhancement effect, resulting in reducing the damping coefficient and damping force while satisfying the performance demand, thereby producing a rational and economical design.

Keywords Inerter · Multistory structure · Structural control · Topological distribution · Damping enhancement

✉ Chao Pan
panchao@ytu.edu.cn

Extended author information available on the last page of the article

1 Introduction

Structural control technology (Housner et al. 1997; Yao 1972) can effectively suppress the dynamic response of civil structures subjected to external excitation. Typical methods of structural control include passive, active, semi-active, and hybrid approaches (Saeed et al. 2015; Soong and Spencer 2002; Spencer and Nagarajaiah 2003; Symans et al. 2008). These structural control methods usually mitigate the structural response by changing the dynamic properties of the structure through additional mechanical elements of mass, damping, or stiffness. Among these three mechanical elements, the damping and stiffness elements are considered as two-terminal elements; that is, the resistive forces are proportional to the relative velocity and displacement between the two terminals. In contrast, a mass element is a single-terminal element that can only be hung on the structure, as in a traditional tuned mass damper (TMD) (Den Hartog 1956). In 1973, Kawamata (1973) developed a type of fluid inerter, under the name of a mass pump, because the term "inerter" had not been defined at that time. Arakaki et al. (1999) developed a rotary damping tube (RDT) that uses a ball-screw mechanism to amplify the effective damping force of a viscous damper. The developed device exhibited an apparent mass effect, which is now referred to as inertance. However, the inertance of the RDT device was not intentionally used because it was not large enough for the control of civil structures. After Saito et al. (2007) and Ikago et al. (2010, 2012a, b, c) proposed the tuned viscous mass damper (TVMD), RDT device was remodeled by attaching cylindrical flywheel to yield a large apparent mass that is enough to control civil structures. Figure 1 shows a two-terminal inerter element. In contrast to a traditional single-terminal mass element, the force of the inerter element is proportional to the relative acceleration between the two terminals:

$$p = m_d\left(\ddot{u}_2 - \ddot{u}_1\right) \tag{1}$$

where p is the output force of the inerter element, m_d is the inertance, and $\ddot{u}_1$ and $\ddot{u}_2$ are the accelerations of the two terminals. An inerter system can combine different types of tuning and energy dissipation enhancement mechanisms in response to the topological configuration of the mechanical elements. There are three basic design for the inerter system that consists of only one inerter, one spring, and one damper: a series layout inerter system (SIS), a series–parallel layout I inerter system (SPIS-I) (Pan and Zhang 2018) or tuned inerter damper (TID) (Lazar et al. 2014), and a series–parallel layout II inerter system (SPIS-II) (Pan and Zhang 2018) or a TVMD (Ikago et al. 2012a, b, c). In addition, there are also other types of inerter systems, such as TMDI (Domenico et al. 2020; Wang and Giaralis 2021).

The mechanism of an inerter can be realized using a ball screw (Ikago et al. 2012a, b, c, 2014; Kida et al. 2012; Nakamura et al. 2017), hydraulics (Nakaminami et al. 2017; Swift et al. 2013; Wang et al. 2011), a gear rack (Makris and Kampas 2016; Saitoh 2012), electromagnetics (Asai et al. 2017a, b; Asai et al. 2017a, b; Gonzalez-Buelga et al. 2015; Gonzalez et al. 2015; Høgsberg and Krenk 2016; Nakamura et al. 2014), etc., of which the

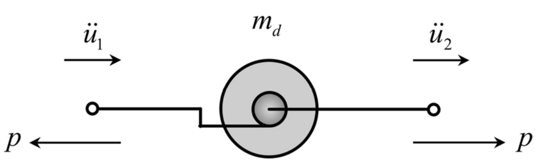

Fig. 1 Two-terminal inerter element

ball screw is used in practical engineering structures (Ikago et al. 2012a, b, c; Nakaminami et al. 2012). A ball screw can amplify axial motion by transforming the relative linear motion between the two terminals into the high-speed rotational motion yielding large inertial and viscous damping torques. The inertial and viscous damping torques are amplified again when they are converted back to translational resistive forces (Ikago et al. 2012a, b, c). Moreover, because the inerter and spring provide a supplemental vibration system resonant to the fundamental natural frequency of the primary structure, the deformation of the damper is also amplified. Therefore, an inerter system can generate large inertial and damping resistive forces with small physical mass and damping coefficient because of the motion amplification effect by the resonant inerter-spring system (Zhang 2014).

In the civil engineering field, vibration control devices with inertial mass enhancement characteristics had already appeared in the 1970s (Kawamata 1973, 1989; Nakamura et al. 1988). Subsequently, the RDT (Arakaki et al. 1999), the gyro mass viscous damper (Kuroda et al. 2000), and the dynamic mass damper was developed (Furuhashi and Ishimaru 2008). At the beginning of this century, Ikago et al. (2010, 2012a, b, c) carried out extensive theoretical and experimental research on inerter systems. A device called the TVMD (Saito et al. 2007, 2008) was proposed, in which a viscous damping element was placed in parallel with an inerter element, and a supporting spring element was connected in series with these two elements. This scheme was the first inerter system applied in practical civil engineering structures (Ogino and Sumiyama 2014; Sugimura et al. 2012). They explicitly use the mass enhancement effect of the inerter element, and also found out the damping enhancement effect of TVMD (Ikago et al. 2010, 2012a, b, c; Saito et al. 2007). However, the fundamental principle of damping enhancement mechanism of TVMD was remained to study at that time.

In civil engineering, building structures remain one of the most promising application areas for inerter systems. Among the basic inerter systems, TVMD (SPIS-II) has proven to be the most technologically sophisticated and practical thus far (Ikago et al. 2012a, b, c; Pan and Zhang 2018). For practical structural design, Ikago et al. (2012a, b, c) used Den Hartog's fixed-point method (Den Hartog 1956) to propose a design method for structures equipped with TVMDs for seismic response control. Lazar et al. (2014) developed an analogous tuning strategy for designing TIDs. These optimal design based on the fixed-point method (Den Hartog 1956) is only applicable to single-degree-of-freedom (SDOF) systems, in which the inherent damping of the primary structures are neglected, and the structural performance demand for the design target is not directly considered. Therefore, Zhang et al. (Pan and Zhang 2018; Pan et al. 2018) conducted a series of investigations on demand-based optimal design for structures equipped with inerter systems considering the inherent damping and cost control of the primary structure. This approach was more comprehensive than the previous methods based on tuning theory. To simplify the design process, Pan and Zhang (2018) further proposed a direct design method for SDOF structures with different inerter systems; in which the stochastic response mitigation ratio was adopted as a design index, and semi-empirical and semi-analytical design formulae were provided for quick calculation, and the OpenSEES was used to verify the design results. Later, Zhang et al. (2020) revealed the damping enhancement mechanism of TVMD and proposed corresponding design strategy for SDOF structure, which is beneficial to fully utilize the energy dissipation performance of the damping element in the TVMD. The previous methods proposed above are mostly based on SDOF structures with inerter systems. However, in practical structural design, higher modal response characteristics cannot be neglected for multistory building structures especially when considering acceleration responses. Ikago et al. (Ikago et al. 2012a, b, c) proposed a method in which a multiple-degree-of-freedom (MDOF) structure was reduced to an equivalent SDOF structure by setting the additional mass of each story proportional to the story stiffness. However, this method retains the drawbacks attributed to the tuning method: the inherent damping is neglected, and the performance demand is not explicitly considered. Taflanidis et al. (2019) proposed a multi-objective optimal design method for MDOF structures equipped with three different inerter systems. The seismic performance of the structure and the control forces of the inerter systems were taken as objective functions, and the seismic performance was evaluated according to reliability-based criteria. However, the allocation method of inerter systems along the height of the multistory structure was not discussed, and the previously utilized methods are numerically complicated for practical design implementation. In addition, the proposed design method did not take the damping enhancement mechanism of TVMD into consideration, which cannot make full use of its performance. Thus, convenient design method for practical MDOF structure with TVMDs based on damping enhancement mechanism needs to be studied in order to comprehensively consider the higher modal response characteristics of the structure and fully utilize the damping enhancement effect of the TVMDs.

In this study, a simple and effective design method is developed for a damped MDOF structure equipped with inerter systems. The demand-oriented design concept demands that the key parameters of inerter systems be directly determined for a target response mitigation ratio. By explicitly utilizing the damping enhancement mechanism, the required damping force, which is closely related to the controlled cost, can be effectively reduced while ensuring vibration control efficiency. The paper is organized as follows. First, the structural governing equations of motion for the damped structure are determined. On the basis of random vibration theory, the stochastic vibration response is obtained by a complex modal analysis and a pseudo excitation method (Lin et al. 2004). The response mitigation ratio is defined as the design index to implement the demand-oriented design philosophy. To maximize the damping enhancement of the inerter system, the design parameters are determined according to the target response mitigation ratio and a preset parameter distribution pattern, which we discuss later. A computer program for designing MDOF structures with inerter systems is developed according to the specified design procedure. The design procedure is demonstrated by application to three example structures with different characteristics. A dynamic time–history analysis with different ground motion excitation is performed to verify the validity and convenience of the proposed method. The damping enhancement effect of the inerter systems designed by the proposed method is compared to an existing method under the same response mitigation ratio.

2 Theoretical basis

A representative inerter system consists of an inerter element, a spring element, and an energy dissipation element. When an inerter system is excited, the inerter-spring system can amplify the deformation of the energy dissipation element to significantly enhance the energy dissipation efficiency (Ikago et al. 2012a, b, c). Therefore, the dynamic response of the primary structure can be suppressed with high efficiency.

Figure 2 shows the inerter system used in this study, where the energy dissipation and inerter elements are arranged in parallel and connected in series with the spring element. Table 1 defines the notations used in this paper.

Fig. 2 Mechanical layout of inerter system adopted in this study (TVMD)

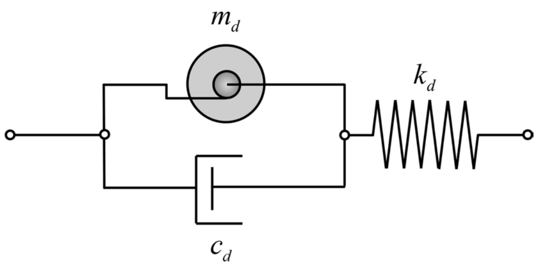

2.1 Governing equations of motion

Figure 3 is the schematic of an MDOF building structure with inerter systems. According to the equilibrium condition, the equations of motion for this structure subjected to ground motion can be expressed as follows:

$$\begin{cases} m_n\ddot{u}_n + F_n + F_{in,n} = -m_n a_g \\ m_{d,n}\ddot{\upsilon}_n + c_{d,n}\dot{\upsilon}_n - k_{d,n}\left(u_n - u_{n-1} - \upsilon_n\right) = 0 \end{cases} \quad n = 1 \sim N, \quad u_0 = 0 \tag{2}$$

where F_n is the force provided by the damping and stiffness of the primary structure, $F_{in,n}$ is the control force of the inerter system, a_g is the acceleration of the ground motion, u_n is the displacement of the nth story relative to the ground, and υ_n is the relative displacement between the two terminals of the inerter element.

For an MDOF building structure with inerter systems, Eq. (2) can be extended to

$$\begin{cases} m_n\ddot{u}_n + F_n + F_{in,n} = -m_n a_g \\ \mu_n m_n\ddot{\upsilon}_n + 2\xi_n\sqrt{m_n k_n}\dot{\upsilon}_n - \kappa_n k_n\left(u_n - u_{n-1} - \upsilon_n\right) = 0 \end{cases}, \; n = 1 \sim N, \quad u_0 = 0 \tag{3}$$

where μ_n, ξ_n, and κ_n are the inertance-mass ratio, the nominal damping ratio of the inerter system, and the stiffness ratio of the inerter system with respect to the primary structure, respectively. These parameters are defined as follows:

$$\mu_n = \frac{m_{d,n}}{m_n}, \quad \xi_n = \frac{c_{d,n}}{2\sqrt{m_n k_n}}, \quad \kappa_n = \frac{k_{d,n}}{k_n} \tag{4}$$

The terms F_n and $F_{in,n}$ can be further expressed as follows:

$$F_n = \begin{cases} c_1\dot{u}_1 + k_1u_1 - c_2\left(\dot{u}_2 - \dot{u}_1\right) - k_2\left(u_2 - u_1\right) & \cdots\ n = 1 \\ c_n\left(\dot{u}_n - \dot{u}_{n-1}\right) + k_n\left(u_n - u_{n-1}\right) - c_{n+1}\left(\dot{u}_{n+1} - \dot{u}_n\right) - k_{n+1}\left(u_{n+1} - u_n\right) & \cdots\ 1 < n < N \\ c_N\left(\dot{u}_N - \dot{u}_{N-1}\right) + k_N\left(u_N - u_{N-1}\right) & \cdots\ n = N \end{cases}$$

$$F_{in,n} = \begin{cases} \kappa_1k_1\left(u_1 - \upsilon_1\right) - \kappa_2k_2\left(u_2 - u_1 - \upsilon_2\right) & \cdots\ n = 1 \\ \kappa_nk_n\left(u_n - u_{n-1} - \upsilon_n\right) - \kappa_{n+1}k_{n+1}\left(u_{n+1} - u_n - \upsilon_{n+1}\right) & \cdots\ 1 < n < N \\ \kappa_Nk_N\left(u_N - u_{N-1} - \upsilon_N\right) & \cdots\ n = N \end{cases} \tag{5}$$

By substituting Eq. (5) into Eq. (3) and rewriting the equations in matrix form, the governing equations of motion can be expressed as follows:

$$\mathbf{M}\ddot{\mathbf{U}} + \mathbf{C}\dot{\mathbf{U}} + \mathbf{K}\mathbf{U} = -\mathbf{M}\mathbf{E}a_g(t) \tag{6}$$

Table 1 Notations

Notation	Definition
p	Output force of inerter element
$m_{d,n}$	Inertance of nth story inerter system
$\ddot{u}_1$	Acceleration at Terminal 1 of inerter
$\ddot{u}_2$	Acceleration at Terminal 2 of inerter
m_n	Mass of nth story
k_n	Stiffness of nth story
h_n	Story height of nth story
c_n	Damping coefficient of nth story
$c_{d,n}$	Damping coefficient of energy dissipation element in inerter system on nth story
$k_{d,n}$	Stiffness of series spring element in inerter system on nth story
F_n	Damping and stiffness force of nth story of primary structure
$F_{in,n}$	Control force of inerter system on nth story
$F_{d,n}$	Damping force of inerter system on nth story
a_g	Acceleration of ground motion
$\tilde{a}_g(\omega, t)$	Acceleration of the pseudo excitation
u_n	Displacement of nth story
$\ddot{u}_n$	Acceleration of nth story
Δu_n	Inter-story drift of nth story
υ_n	Relative displacement between two terminals of inerter
$\dot{\upsilon}_n$	Relative velocity between two terminals of inerter
$\ddot{\upsilon}_n$	Relative acceleration between two terminals of inerter
μ	Inertance-mass ratio
ξ	Nominal damping ratio of inerter system
κ	Stiffness ratio of inerter system with respect to primary structure
ω	Circular frequency of harmonic excitation
$\omega_{p,i}$	The ith fundamental circular frequency of the primary structure
ζ_i	The ith damping ratio of the primary structure
A_g	Amplitude of harmonic excitation
$S_g(\omega)$	Power spectral density function of excitation
σ_U^2	Mean square of stochastic displacement response of primary MDOF structure
γ_n	Response mitigation ratio
$\gamma_{t,n}$	Target response mitigation ratio
β	Constant coefficient of parameter distribution
θ_n	Inter-story drift angle of nth story
$\tilde{\theta}_n$	Normalized inter-story drift angle of nth story
$\theta_{\max}$	Maximization of inter-story drift angle of the controlled structure
$\theta_{o,\max}$	Maximization of inter-story drift angle of the original structure
$[\theta]$	Inter-story drift limit
η	Seismic capacity redundancy of structure
ψ	Parameter distribution index
$\boldsymbol{\varphi}_{part,i}$	The ith participation mode vector of the structure
α	Ratio of damper deformation to whole inerter system deformation

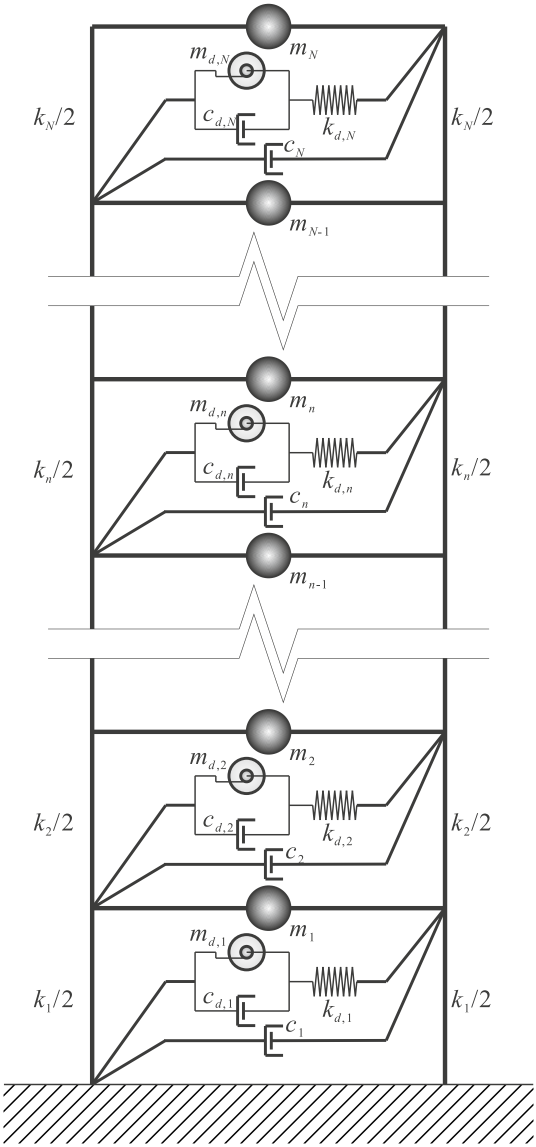

Fig. 3 Schematic of an MDOF building structure equipped with inerter systems

where

$$\mathbf{U} = \begin{pmatrix} u_1 & v_1 & u_2 & v_2 & \cdots & u_N & v_N \end{pmatrix}^{\mathrm{T}} \tag{7}$$

$$\mathbf{E} = \begin{pmatrix} 1 & 0 & 1 & 0 & \cdots & 1 & 0 \end{pmatrix}^{\mathrm{T}} \tag{8}$$

$$\mathbf{M} = \mathrm{diag}\left(m_1, \mu_1 m_1, m_2, \mu_2 m_2, \cdots, m_N, \mu_N m_N\right) \tag{9}$$

$$
\mathbf{C}=\begin{pmatrix}
c_1+c_2 & 0 & -c_2 & & & & & \\
 & 2\xi_1\sqrt{m_1k_1} & & & & & & \\
 & & c_2+c_3 & 0 & -c_3 & & & \\
 & & & 2\xi_2\sqrt{m_2k_2} & & & & \\
 & & & & \ddots & & & \\
 & & \textbf{symmetry} & & & c_{N-1}+c_N & 0 & -c_N \\
 & & & & & & 2\xi_{N-1}\sqrt{m_{N-1}k_{N-1}} & \\
 & & & & & & & c_N \\
 & & & & & & & & 2\xi_N\sqrt{m_Nk_N}
\end{pmatrix} \tag{10}
$$

$$
\mathbf{K}=\begin{pmatrix}
\sum_{q=1}^{2}(1+\kappa_q)k_q & -\kappa_1k_1 & -(1+\kappa_2)k_2 & \kappa_2k_2 & & & & \\
 & \kappa_1k_1 & & & & & & \\
 & & \sum_{q=2}^{3}(1+\kappa_q)k_q & -\kappa_2k_2 & -(1+\kappa_3)k_3 & \kappa_3k_3 & & \\
 & & & \kappa_2k_2 & & & & \\
 & & & & \ddots & & & \\
 & & \textbf{symmetry} & & \sum_{q=N-1}^{N}(1+\kappa_q)k_q & -\kappa_{N-1}k_{N-1} & -(1+\kappa_N)k_N & \kappa_Nk_N \\
 & & & & & \kappa_{N-1}k_{N-1} & & \\
 & & & & & & (1+\kappa_N)k_N & -\kappa_Nk_N \\
 & & & & & & & \kappa_Nk_N
\end{pmatrix} \tag{11}
$$

2.2 Solution of stochastic response

To determine the optimal design of inerter systems to be incorporated into an N-story MDOF structure, a random vibration analysis needs to be performed on the uncontrolled system beforehand. The dynamic characteristics of an MDOF structure can be obtained through modal analysis. For the damped MDOF structure considered in this study, the damping of the system is non-proportional. Therefore, the modal damping matrix and modal stiffness matrix are not simultaneously diagonalized in the classical manner, which results in complex eigenvalues and modes (Veletsos and Ventura 1986; Yang et al. 2003). Foss's method (Ohtori et al. 2004) or the equivalent state-space method (Li and Hu 2016) can be used to convert Eq. (6) into 4 N first-order matrix state-space equations:

$$
\mathbf{A}\dot{\mathbf{Y}}+\mathbf{B}\mathbf{Y}=\mathbf{F}a_g(t) \tag{12}
$$

where

$$
\mathbf{A}=\begin{pmatrix}\mathbf{O} & \mathbf{M}\\ \mathbf{M} & \mathbf{C}\end{pmatrix}_{4N\times4N},\quad \mathbf{B}=\begin{pmatrix}-\mathbf{M} & \mathbf{O}\\ \mathbf{O} & \mathbf{K}\end{pmatrix}_{4N\times4N},\quad \mathbf{F}=\begin{pmatrix}\mathbf{O}\\ -\mathbf{ME}\end{pmatrix}_{4N\times1},\quad \mathbf{Y}=\begin{pmatrix}\dot{\mathbf{U}}\\ \mathbf{U}\end{pmatrix}_{4N\times1} \tag{13}
$$

If the external excitation is assumed to be harmonic, then

$$
a_g(t)=A_ge^{i\omega t}=A_ge^{\lambda t} \tag{14}
$$

The response of the MDOF structure can then be expressed as

$$\mathbf{Y}(t)=\begin{pmatrix} \dot{\mathbf{U}}(t) \\ \mathbf{U}(t) \end{pmatrix} = \begin{pmatrix} \lambda\varphi \\ \varphi \end{pmatrix} e^{\lambda t} = \boldsymbol{\varphi} e^{\lambda t} \tag{15}$$

Thus, the eigenvalue problem of Eq. (12) can be expressed as

$$(\mathbf{A}\lambda + \mathbf{B})\begin{Bmatrix} \lambda\varphi \\ \varphi \end{Bmatrix} = 0 \tag{16}$$

The eigenvalues $\boldsymbol{\lambda}$ and eigenvectors $\boldsymbol{\Phi}$ of Eq. (16) can be calculated as 2 N complex conjugate pairs:

$$\begin{aligned} \boldsymbol{\lambda} &= \left(\lambda_1, \overline{\lambda}_1, \lambda_2, \overline{\lambda}_2, \cdots, \lambda_{2N-1}, \overline{\lambda}_{2N-1}, \lambda_{2N}, \overline{\lambda}_{2N}\right)^{\mathrm{T}} \\ \boldsymbol{\Phi} &= \left(\boldsymbol{\varphi}_1, \overline{\boldsymbol{\varphi}}_1, \boldsymbol{\varphi}_2, \overline{\boldsymbol{\varphi}}_2, \cdots, \boldsymbol{\varphi}_{2N-1}, \overline{\boldsymbol{\varphi}}_{2N-1}, \boldsymbol{\varphi}_{2N}, \overline{\boldsymbol{\varphi}}_{2N}\right) \end{aligned} \tag{17}$$

where () denotes the complex conjugate. The ith fundamental circular frequency $\omega_{p,i}$ of the structure system can be obtained as follows:

$$\omega_{p,i} = \left|\lambda_i\right| = \left|\overline{\lambda}_i\right| \tag{18}$$

The corresponding damping ratio ζ_i of the structure system can be calculated as follows (Igusa and Kiureghian 1985; Ikago et al. 2012a, b, c; Veletsos and Ventura 1986):

$$\zeta_i = -\frac{\mathrm{Re}\left[\lambda_i\right]}{\left|\lambda_i\right|} = -\frac{\mathrm{Re}\left[\overline{\lambda}_i\right]}{\left|\lambda_i\right|} \tag{19}$$

By using the transformation $\mathbf{Y}(t) = \boldsymbol{\Phi}\mathbf{Z}(t)$, Eq. (12) can then be reduced to 4 N decoupled modal equations:

$$\mathbf{A}_{\mathbf{r}}\dot{\mathbf{Z}}(t)+\mathbf{B}_{\mathbf{r}}\mathbf{Z}(t)= \boldsymbol{\Phi}^{\mathrm{T}}\mathbf{F}a_g(t) \tag{20}$$

where $\mathbf{Z}(t)$ is the modal coordinate. Alternatively,

$$\dot{\mathbf{Z}}(t) - \boldsymbol{\Lambda}\mathbf{Z}(t)= \mathbf{R}a_g(t), \tag{21}$$

where

$$\begin{cases} \mathbf{A}_{\mathbf{r}} = \boldsymbol{\Phi}^{\mathrm{T}}\mathbf{A}\ \boldsymbol{\Phi} \\ \mathbf{B}_{\mathbf{r}} = \boldsymbol{\Phi}^{\mathrm{T}}\mathbf{B}\ \boldsymbol{\Phi} = -\lambda\mathbf{A}_{\mathbf{r}} \\ \boldsymbol{\Lambda} = \mathrm{diag}\left(\lambda_1, \overline{\lambda}_1, \lambda_2, \overline{\lambda}_2, \cdots, \lambda_{2N-1}, \overline{\lambda}_{2N-1}, \lambda_{2N}, \overline{\lambda}_{2N}\right) \\ \mathbf{R} = \boldsymbol{\Phi}^{\mathrm{T}}\mathbf{F}/\mathbf{A}_{\mathbf{r}} = \mathrm{diag}\left(r_1, \overline{r}_1, r_2, \overline{r}_2, \cdots, r_{2N-1}, \overline{r}_{2N-1}, r_{2N}, \overline{r}_{2N}\right) \end{cases} \tag{22}$$

The components from the odd rows in the bottom half of $\boldsymbol{\Phi}$ can be extracted to construct a new matrix as follows:

$$P = \left(\phi_1,\ \overline{\phi}_1,\ \phi_2,\ \overline{\phi}_2,\ \cdots\ ,\phi_{2N-1},\ \overline{\phi}_{2N-1},\ \phi_{2N},\ \overline{\phi}_{2N}\right)_{N\times 4N} \tag{23}$$

The mode participation matrix can be obtained as follows:

$$\boldsymbol{\Phi}_{part} = \left(\boldsymbol{\varphi}_{part,1}, \overline{\boldsymbol{\varphi}}_{part,1}, \boldsymbol{\varphi}_{part,2}, \overline{\boldsymbol{\varphi}}_{part,2}, \cdots, \boldsymbol{\varphi}_{part,2N-1}, \overline{\boldsymbol{\varphi}}_{part,2N-1}, \boldsymbol{\varphi}_{part,2N}, \overline{\boldsymbol{\varphi}}_{part,2N}\right)_{N\times 4N}, \tag{24}$$

where $\boldsymbol{\varphi}_{part,i}$ is the ith participation mode vector of the structure that can be calculated as

$$\boldsymbol{\varphi}_{part,i} = r_i \lambda_i \phi_i, \quad \overline{\boldsymbol{\varphi}}_{part,i} = \overline{r}_i \overline{\lambda}_i \overline{\phi}_i \tag{25}$$

Thus, the vibration problem of an MDOF structure can be decoupled into the vibrations of a set of independent SDOF systems. The stochastic response of the decoupled system can be obtained based on random vibration theory. In this study, the pseudo excitation method (Lin et al. 2004; Xu et al. 1999; Zhang and Xu 1999) is used to solve the stochastic response. The external excitation $a_g(t)$ is assumed to be a stationary random process, and the input power spectrum of $a_g(t)$ is assumed to be $S_g(\omega)$. Then, the acceleration of the pseudo excitation (Lin et al. 2004) of the ground motion can be formulated as follows:

$$\tilde{a}_g(\omega, t) = \sqrt{S_g(\omega)} \cdot e^{i\omega t} \tag{26}$$

Based on Eqs. (22) and (26), Eq. (21) can be solved to yield

$$Z_n(\omega, t) = \frac{r_n}{i\omega - \lambda_n} \sqrt{S_g(\omega)} \cdot e^{i\omega t} = Z_n(\omega) \cdot e^{i\omega t} \tag{27}$$

Consequently,

$$\mathbf{Y}(\omega, t) = \boldsymbol{\Phi}\mathbf{Z}(t) = \sum_{n=1}^{4N} \boldsymbol{\varphi}_n \cdot \frac{r_n}{i\omega - \lambda_n} \sqrt{S_g(\omega)} \cdot e^{i\omega t} = \begin{pmatrix} \dot{\mathbf{U}}(\omega) \\ \mathbf{U}(\omega) \end{pmatrix} \cdot e^{i\omega t} \tag{28}$$

The power spectral density of the structural dynamic response can be conveniently calculated as follows:

$$\mathbf{S}_U(\omega) = \overline{\mathbf{U}}(\omega)\mathbf{U}(\omega) \tag{29}$$

The mean square displacement response of the MDOF structure can then be calculated as

$$\sigma_U^2 = \int_{-\infty}^{\infty} \mathbf{S}_U(\omega)\, d\omega \tag{30}$$

3 Demand-oriented design based on damping enhancement strategy

3.1 Design concept

3.1.1 Demand oriented design index

Here, we define the demand-oriented design index as follows:

$$\gamma = \frac{\text{Response of structure with inerter system}}{\text{Response of uncontrolled original structure}} \tag{31}$$

The target response mitigation ratio γ_t can be determined according to the performance demand after the initial performance evaluation analysis on the uncontrolled original structure and is defined as

$$\gamma_t = \frac{\text{Target performance limit}}{\text{Response of uncontrolled original structure}} \tag{32}$$

An effective design should satisfy the following performance demand:

$$\gamma \le \gamma_t \tag{33}$$

3.1.2 Topological damping enhancement: Rational parameter distribution patterns

As previously mentioned, an inerter system is generally composed of an inerter element, an energy dissipation element, and a spring element. The parameters of these elements must be determined in the design of the inerter system. In this study, three dimensionless parameters are adopted as the key design parameters of the inerter system: the inertance-mass ratio μ_n, the nominal damping ratio ξ_n, and the stiffness ratio κ_n. For an N-story MDOF structure with inerter systems, 3 N parameters need to be determined $(\mu_1, \mu_2, \cdots \mu_N, \xi_1, \xi_2, \cdots \xi_N, \kappa_1, \kappa_2, \cdots \kappa_N)$.

Given an excitation with the power spectral density of $S_g(\omega) = S_0$, the response mitigation ratio is derived as follows:

$$\gamma = f(\mu_1, \mu_2, \cdots \mu_N, \xi_1, \xi_2, \cdots \xi_N, \kappa_1, \kappa_2, \cdots \kappa_N) \quad \cdots \quad n = 1, 2, \cdots, N \tag{34}$$

In practical design, it is not necessary to install vibration control devices on all of the stories of a structure. Equipping stories with larger inter-story drifts with more damping devices is a more effective means of controlling responses of the structure, realizing the damping enhancement topologically. In this study, considering the characteristics of an MDOF structure, the distributions of the design parameters are assumed to be positively correlated with the story drifts to simplify the optimization process, as shown in Eq. (35). Thus, the design parameters of the inerter system on weak stories shall increase correspondingly:

$$\mu_n = \mu\beta\tilde{\theta}_n^{\psi}, \quad \xi_n = \xi\beta\tilde{\theta}_n^{\psi}, \quad \kappa_n = \kappa\beta\tilde{\theta}_n^{\psi}, \tag{35}$$

where β is a constant coefficient that can be determined according to the elastic strain energy of the primary structure:

$$\beta = \frac{\sum_{n=1}^{N} k_n h_n^2 \tilde{\theta}_n^{2+\psi}}{\sum_{n=1}^{N} k_n h_n^2 \tilde{\theta}_n^2} \tag{36}$$

where k_n and h_n are the story stiffness and story height of the primary structure respectively. The term $\tilde{\theta}_n$ is the normalized inter-story drift angle of the nth story:

$$\tilde{\theta}_n = \frac{\theta_n}{\theta_{\max}} = \frac{\Delta u_n / h_n}{\max\left(\Delta u_n / h_n\right)} \tag{37}$$

where Δu_n is the inerterstory drift of the nth story. The term $\theta_{\max}$ is the maximum values of $\Delta u_n / h_n$. The parameter distribution index ψ in Eq. (35) refers to the positive correlation degree between the parameters and the story drift ($\psi \geq 1$). In practical design, the value of ψ can be determined empirically via trial calculations. Thus, the design parameters of an MDOF structure with inerter systems are reduced into three unknown parameters (μ, ξ, and κ) for the optimization process. It should be noted that the parameter distributions of the design parameters μ, ξ, and κ are the same shape according to the Eq. (35).

3.1.3 Fundamental damping enhancement

As was discussed in Sect. 2, the inerter element can produce amplified inertance and enlarge the effective deformation of the connected damping element, thereby amplifying energy dissipation efficiency (Ikago et al. 2012a, b, c). Figure 4 illustrates the damping enhancement effect. To evaluate the damping enhancement effect quantitatively, the damping deformation enhancement ratio α of the inerter system is defined as follows:

$$\alpha = \frac{\text{Deformation of damping element of inerter system}}{\text{Deformation of the inerter system}} \tag{38}$$

In line with the damping enhancement mechanism, the parameters of the inerter systems are determined by maximizing the deformation of the damping element. According to the damping enhancement equation proposed by Zhang et al. (Zhang, Zhao, Pan, Ikago and Xue 2020), the maximization of damping element deformation is equivalent to the minimization of nominal damping coefficient ξ based on a target response mitigation ratio γ_t. Therefore, the damping coefficient ξ can be considered as the objective function in the design following the damping enhancement effect principle.

3.2 Design procedure

In an ideal design, it is insufficient to minimize the dynamic response while neglecting the cost. A rational approach strikes a balance between the performance and economic demands. Therefore, for an MDOF building structure equipped with inerter systems, the

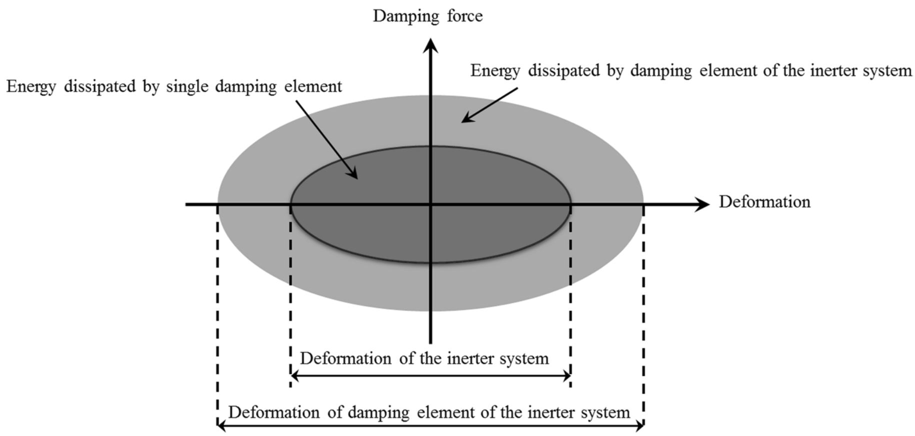

Fig. 4 Schematic representation of damping enhancement effect (Ikago et al. 2012a, b, c)

design parameters μ, ξ, and κ should be determined to achieve the desired performance while providing economy. In this study, the response demand of a structure equipped with inerter systems is reflected by the response mitigation ratio γ, and the target response mitigation ratio γ_t is considered as the constraint. To maximizing the damping enhancement effect of the inerter system, the nominal damping ratio ξ needs to be minimized in the design procedure. In addition, the control cost is also considered because the minimization of the nominal damping ratio ξ which influences the cost of the damping element in the inerter system. However, it should be stated that the proposed method just considered the control cost from an aspect, there are still other complex factors effecting the economic cost of the structure in practical engineering.

On the basis of the discussion above, the design of an MDOF structure with inerter systems can be expressed as follows:

$$\begin{cases} \text{minimize} & \xi \\ \text{subject to} & \gamma = \dfrac{\theta_{\max}}{\theta_{o,\max}} = \gamma_t = \dfrac{[\theta]}{\eta\theta_{o,\max}} \end{cases} \tag{39}$$

where η is the seismic capacity redundancy (Hao et al. 2017) of the structure. Compared with traditional design methods (such as the fixed-point design) this design philosophy has more explicit physical meaning, that is, satisfying the required performance demand with smaller damping coefficient ξ. A computer program is developed to solve Eq. in MATLAB (Mathworks 2017) to obtain optimal design of the inerter system incorporated into an MDOF structure. The optimal toolbox of MATLAB is used to find an optimum solution to the optimization problem above. Figure 5 is a flowchart for the demand-oriented optimal design of an MDOF structure with inerter systems.

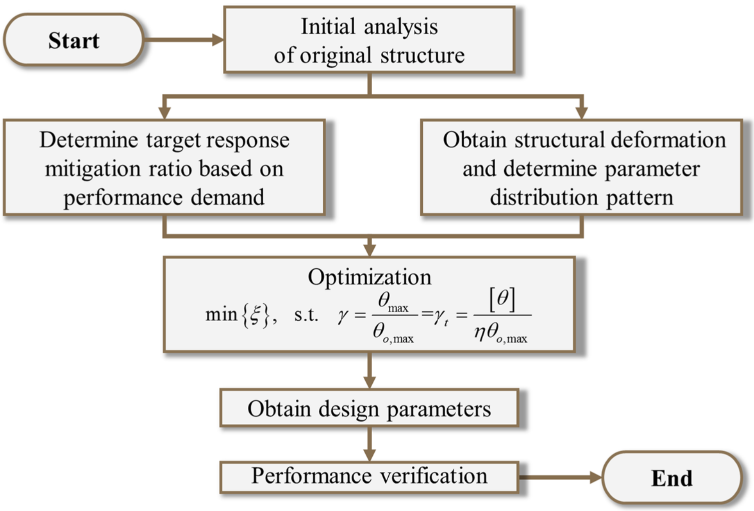

Fig. 5 Flowchart for demand oriented optimal design of an MDOF structure with inerter systems

4 Case design

In this section, three elastic benchmark structures having different characteristics are employed to exemplify the generality and effectiveness of the proposed design method. Comparison between the costs of the designs derived by the proposed and conventional methods illustrates the superiority of the proposed method.

4.1 Model with distinctly non-uniform story drifts

Model 1 (M1) is a shear-type structure with distinctly non-uniform story drifts (Chopra 2012). Table 2 lists the model information, and the inherent damping ratio of the primary structure for the first mode is 5%. The natural periods of the first three modes of M1 are presented in Table 3.

The target response mitigation ratio is set to $\gamma_t = 0.7$ according to the initial analysis of the primary structure. On the basis of the parameter distribution pattern proposed in Eq. (35), increasing the distribution index ψ decreases the optimal solutions for μ, ξ, and κ to some extent. This result is obtained because a greater positive correlation degree between the parameter and story drift means that more damping devices are to be allocated to stories with larger story drifts. This result also means that the same response mitigation effect can be achieved with smaller parameter values by selecting an appropriate distribution index ψ. Considering structural reliability, the value of ψ cannot be too large, otherwise the parameters will be too concentrated. On the basis of a series of trial calculations using different values of ψ from 1 ~ 5, the empirical value of $\psi = 3$ is recommended for the design of M1. The optimal design parameters are listed in Table 4.

On the basis of the eigenvalue analysis of the controlled structure that was presented in Sect. 2.2, Table 5 compares the modal periods and damping ratios of the original and controlled structures. Adding the inerter system splits the first mode of the uncontrolled structure into two modes: the 1st and 11th modes in the controlled structure. Thus, the periods of the 1st and 11th modes of the structure containing the inerter system are close to each other. The periods of the 2nd to 10th modes that are attributed to the local fundamental natural periods of the inerter system itself are close to each other as well. The damping ratios of the 1st to 11th modes of the controlled structure increase with the addition of the inerter system, whereas the 12th and 13th modes are almost unchanged and correspond to the 2nd and 3rd modes of the original structure, respectively (Ikago et al. 2012a, b, c). The corresponding participation mode vectors $\boldsymbol{\varphi}_{part,i}$ are depicted in Fig. 6.

Table 2 Model information (M1)

Floor number n	Story height h (mm)	Mass m_n (ton)	Stiffness k_n (kN/m)
1–10	3000	20	2700

Table 3 Modal periods of the primary structure (M1)

Mode	Period (s)
1st	3.62
2nd	1.22
3rd	0.74

Table 4 Optimal design data of M1 with inerter systems

Floor Number n	μ_n	$m_{d,n}$ (ton)	ξ_n	$c_{d,n}$ (kNs/m)	κ_n	$k_{d,n}$ (kN/m)
10	0.012	0.2	0.0003	0.1	0.0003	0.9
9	0.093	2	0.0023	1	0.0024	7
8	0.293	6	0.0072	3	0.0077	21
7	0.634	13	0.0156	7	0.0166	45
6	1.107	22	0.0273	13	0.0290	78
5	1.680	34	0.0413	19	0.0440	119
4	2.295	46	0.0565	26	0.0601	162
3	2.884	58	0.0710	33	0.0755	204
2	3.374	67	0.0830	39	0.0884	239
1	3.699	74	0.0911	42	0.0969	262

Table 5 Modal periods and damping ratio of original and controlled structures

Original structure			Controlled structure with inerter system		
Mode	Period	Damping ratio	Mode	Period	Damping ratio
1	3.62	0.05	**1**	**3.93**	**0.108**
			2	3.54	0.163
			3	3.52	0.162
			4	3.49	0.160
			5	3.46	0.158
			6	3.44	0.156
			7	3.41	0.154
			8	3.39	0.153
			9	3.39	0.152
			10	3.38	0.152
			11	**3.13**	**0.100**
2	1.22	0.15	12	1.20	0.145
3	0.74	0.24	13	0.75	0.239

The bold content contributes to stress the change of the modal period of the structure with inerter system compared to the original structure

Figure 7 shows the analysis results of M1 under the excitation of Kanai-Tajimi spectrum $S_g(\omega)$. Figure 8 illustrates the parameter distribution pattern of the structure. It can be seen directly that stories having large displacements are equipped with larger parameters. The displacement power spectral density function of the 1st story is shown in Fig. 9. The performance of M1 is effectively improved with the inerter system, especially for the lower stories with larger story drifts. Table 6 lists the damping deformation enhancement ratios α of the inerter systems. It is shown that the deformation of the damping element is effectively magnified by the inerter systems, in accordance with the damping enhancement strategy.

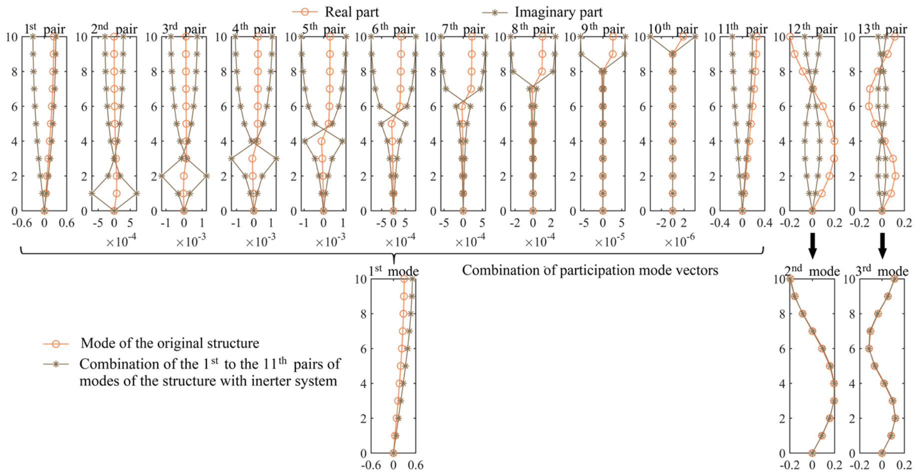

Fig. 6 Participation mode vectors of M1

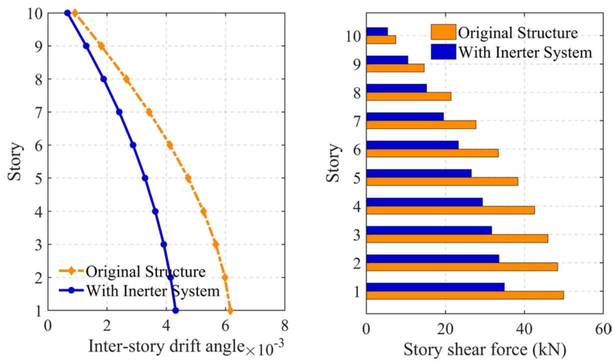

Fig. 7 Inter-story drift angles and story shear forces (M1)

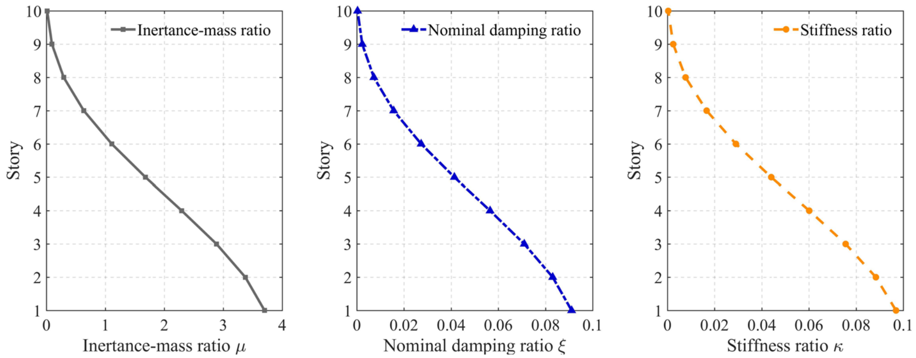

Fig. 8 Parameter distribution (M1)

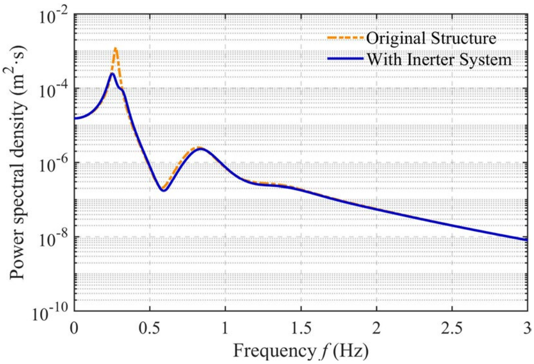

Fig. 9 Displacement power spectral density function (M1: 1st story)

Table 6 Damping deformation enhancement ratio α of inerter system

Floor number n	1	2	3	4	5	6	7	8	9	10
α	2.37	2.40	2.43	2.46	2.48	2.48	2.47	2.46	2.44	2.42

4.2 Steel frame structure

To investigate the feasibility of applying method to practical structures, a nine-story frame structure is utilized in this section. The lateral load-resisting system of the structure is composed of steel perimeter moment-resisting frames (M2). This study focuses on the in-plane (two-dimensional) analysis of the structure, and a single MRF is employed to verify the design. The columns and beams of the MRF are in the form of wide flanges. The columns and beams are made of steel with yielding strengths of 345 and 248 MPa, respectively. Figure 10 shows the section dimensions of the columns and beams.

In order to design the inerter systems by the proposed method, the two-dimensional model of the steel frames was established in OpenSEES (McKenna et al. 2000), and the pushover analysis was carried out to obtain the story stiffness of M2. The story mass of M2 can be calculated according to the gravity and loads of it. The inherent damping ratio of the primary

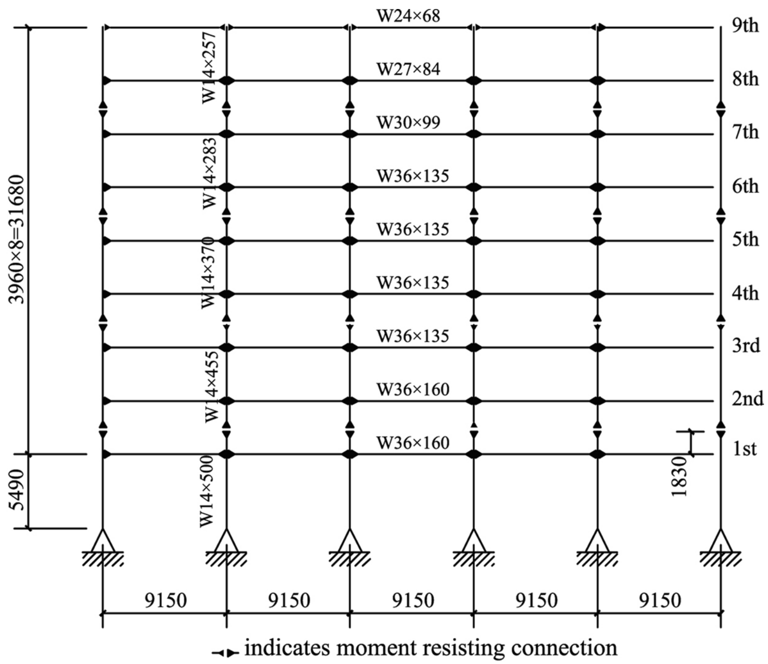

Fig. 10 Model 2 (M2): nine-story steel frame structure

Table 7 Model information (M2)

Floor number n	Story height h (mm)	Story mass m_n (ton)	Story stiffness k_n (kN/m)
9	3960	534.6	58,205.9
8	3960	494.2	84,968.9
7	3960	494.2	117,202.4
6	3960	494.2	153,412.9
5	3960	494.2	168,236.9
4	3960	494.2	178,923.8
3	3960	494.2	198,710.0
2	3960	494.2	212,966.2
1	5490	504.7	177,701.5

Table 8 Modal periods of primary structure (M2)

Mode	Period (s)
1st	2.06
2nd	0.81
3rd	0.50

Table 9 Optimal design of inerter systems incorporated into M2

Floor number n	μ_n	$m_{d,n}$(ton)	ξ_n	$c_{d,n}$(kNs/m)	κ_n	$k_{d,n}$(kN/m)
9	2.469	1320	0.0286	319	0.0750	4363
8	4.810	2377	0.0557	722	0.1460	12,407
7	4.954	2448	0.0574	873	0.1504	17,627
6	4.262	2106	0.0494	859	0.1294	19,851
5	5.173	2557	0.0599	1092	0.1570	26,421
4	6.050	2990	0.0701	1317	0.1837	32,861
3	5.632	2783	0.0652	1293	0.1710	33,975
2	5.403	2670	0.0626	1284	0.1640	34,931
1	3.869	1953	0.0448	849	0.1175	20,874

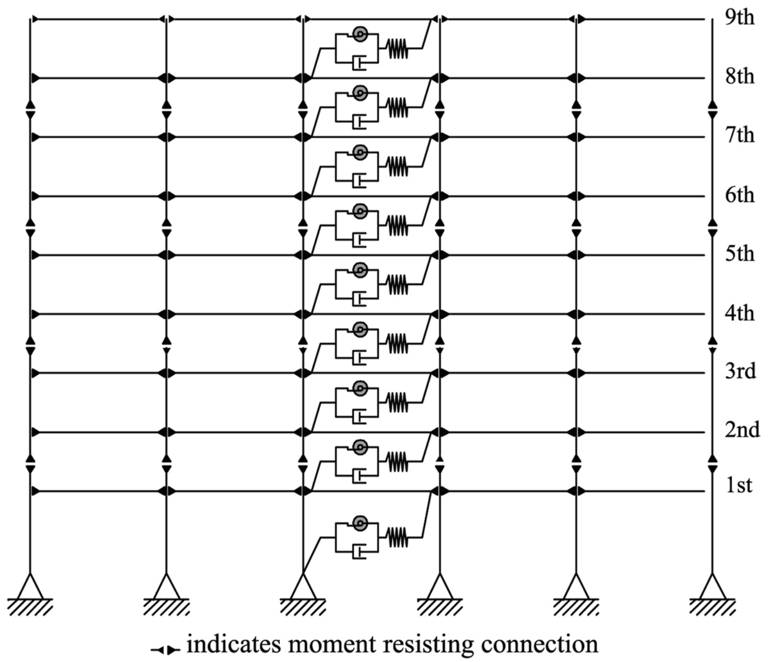

Fig. 11 Elevation of inerter system arrangement

structure is 4% (China Ministry of Housing and Urban–Rural Construction 2015). Table 7 lists the model information, and the model periods of the structure are presented in Table 8.

The target response mitigation ratio is set to $\gamma_t = 0.6$ according to the initial analysis of the primary structure. The parameter distribution index is $\psi = 3$ according to the trial calculation results. Using the method proposed in this study, the optimal design parameters of the inerter system are listed in Table 9. Although the inertance in each story is much larger than the story mass of the primary structure, the required physical mass of inerter can be reduced by thousands of times owing to the mass enhancement effect.

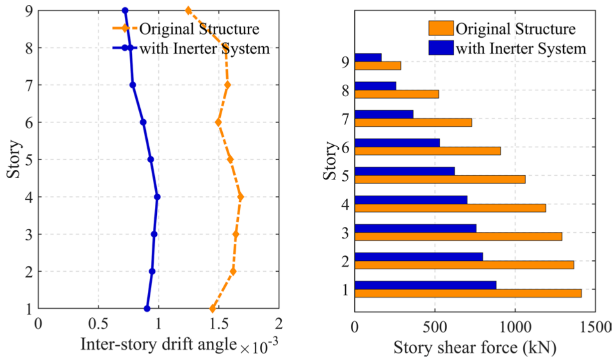

Fig. 12 Inter-story drift angles and story shear forces (M2)

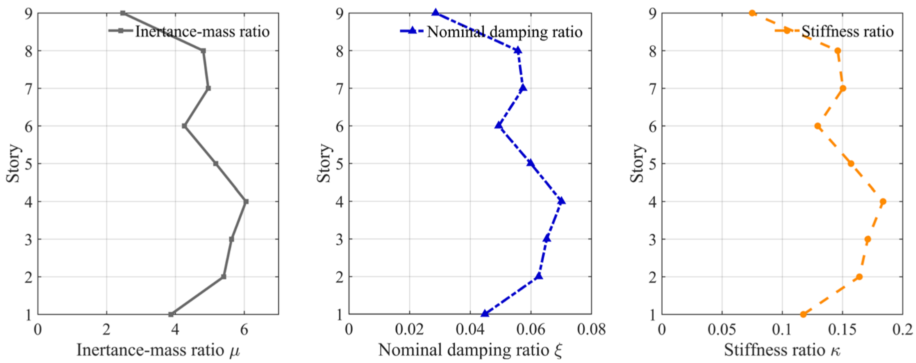

Fig. 13 Parameter distribution (M2)

The installation of the inerter system (TVMD) on the steel frame structure is shown in Fig. 11.

Figure 12 is the inter-story drift angles and story shear forces of M2 subjected to the excitation of $S_g(\omega)$. Figure 13 is the parameter distribution of M2. It is shown in the two figures that the response of original structure has been controlled. To further demonstrate the effectiveness of the proposed design method, the two-dimensional model of the steel frames established in OpenSEES was employed to carry out several time-history dynamic analyses to verify the design results. A white noise and two ground motion records (PGA = 0.1g) were employed in the time history analysis. Figure 14 shows the time–history response of the top story of M2. The dynamic responses of the structures are effectively mitigated, and the response mitigation ratios are close to the value calculated via the combined complex mode superposition and pseudo-excitation method; thus, the validity and efficiency of the demand-oriented optimal design method are confirmed.

4.3 Comparison case: Benchmark model

In this section, a 10-story benchmark structure (hereinafter referred to as M3) provided by the Japan Society of Seismic Isolation(Japan Society of Seismic Isolation 2007) is utilized to conduct a comparison analysis. Detailed information of M3 is listed in Table 10. The

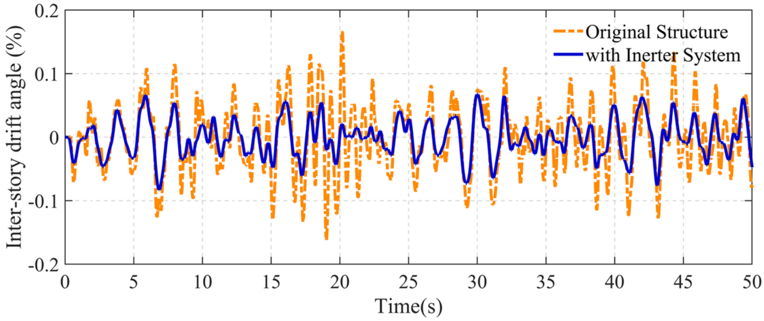

(a) White noise excitation (Response mitigation ratio: 0.60)

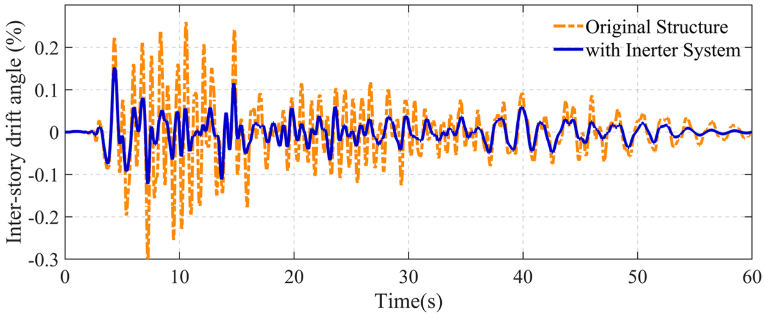

(b) Ground motion record - Taft (Response mitigation ratio: 0.60)

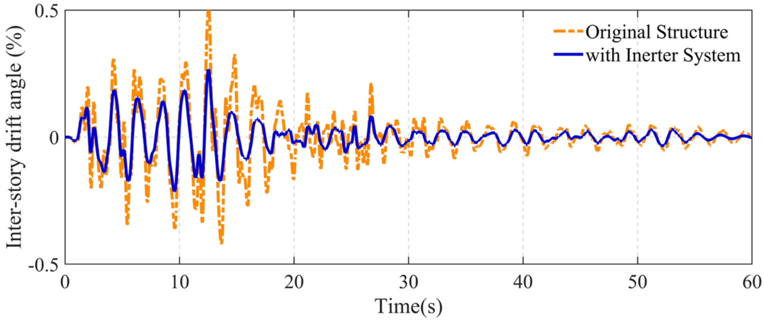

(c) Ground motion record – El Centro (Response mitigation ratio: 0.53)

Fig. 14 Time–history response of top story of M2 ($\gamma_t = 0.60$)

inherent damping ratio of the primary structure is 2%. Table 11 lists the periods of the first three modes.

The proposed method is compared with the fixed-point method (Ikago et al. 2012a, b, c) to illustrate its superior performance in employing damping enhancement effect. The response mitigation ratio of M3 incorporated with TVMD systems using the fixed-point method (Ikago et al. 2012a, b, c) can be estimated as 0.45. Thus, the target response mitigation ratio is set to be the same value of $\gamma_t = 0.45$ in this design. The parameters of inerter system designed by the proposed method are listed in Table 12. The optimal parameter sets are obtained for the

Table 10 Model information (M3)

Floor number n	Story height h (mm)	Mass m_n (ton)	Stiffness k_n (kN/m)
10	4000	875	158,550
9	4000	649	180,110
8	4000	656	220,250
7	4000	660	244,790
6	4000	667	291,890
5	4000	670	306,160
4	4000	676	328,260
3	4000	680	383,020
2	4000	682	383,550
1	6000	700	279,960

Table 11 Modal periods of primary structure (M3)

Modals	Period (s)
1^{st}	2.01
2^{nd}	0.76
3^{rd}	0.46

parameter distribution index $\psi = 1$ because there is no obvious change in the story drifts of the primary structure. The comparison of damping coefficients and damping forces between the two methods are listed in Table 13. Maximizing damping deformation by the proposed method largely reduces the damping forces over those obtained using the fixed-point method. Therefore, the cost of an inerter system in practical application can be effectively reduced when the excitation is white noise. Figure 15 shows the inter-story drift angles and the story shear forces of M3 under the excitation $S_g(\omega)$. In this figure, the parameters of inerter system-1 are designed by the proposed method in this manuscript, and the parameters of inerter system-2 are designed by the fixed-point method. The parameter distribution pattern is shown in Fig. 16. It can be seen in the Fig. 15 that the story drifts and the story shear forces are

Table 12 Optimal design parameters of M3 with inerter systems

Floor number n	μ_n	$m_{d,n}$(ton)	ξ_n	$c_{d,n}$(kNs/m)	κ_n	$k_{d,n}$(kN/m)
10	2.246	1965	0.0519	1222	0.0631	10,007
9	3.338	2166	0.0771	1666	0.0938	16,891
8	3.743	2455	0.0864	2078	0.1052	23,162
7	4.185	2762	0.0966	2457	0.1176	28,787
6	4.116	2745	0.0950	2652	0.1157	33,759
5	4.426	2967	0.1022	2928	0.1244	38,077
4	4.520	3056	0.1044	3110	0.1270	41,693
3	4.140	2815	0.0956	3086	0.1163	44,556
2	4.333	2955	0.1000	3236	0.1217	46,696
1	4.074	2852	0.0941	2634	0.1145	32,047

Table 13 Comparison of results obtained using proposed method and fixed-point method

Proposed method		Fixed-point method (Ikago et al. 2012a, b, c)		Reduction of damping force
$c_{d,n}$(kNs/m)	$F_{d,n}$(kN)	$c^*_{d,n}$(kNs/m)	$F^*_{d,n}$(kN)	$\left(F^*_{d,n} - F_{d,n}\right)/F^*_{d,n}$
1222	45	2353	155	70.97% (↓)
1666	159	2673	262	39.31% (↓)
2078	262	3269	360	27.22% (↓)
2457	363	3633	447	18.79% (↓)
2652	410	4332	523	21.60% (↓)
2928	489	4544	588	16.84% (↓)
3110	536	4872	641	16.38% (↓)
3086	499	5684	684	27.05% (↓)
3236	540	5692	715	24.48% (↓)
2634	592	4155	736	19.57% (↓)

Fig. 15 Inter-story drift angles and story shear forces

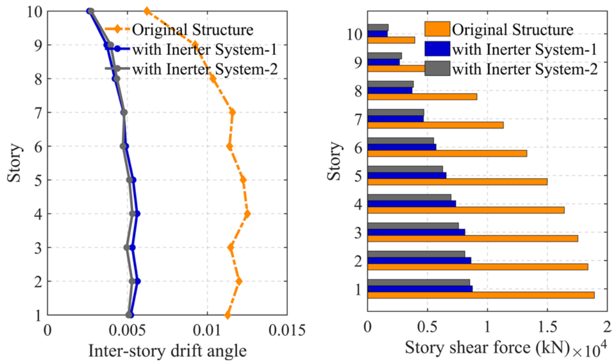

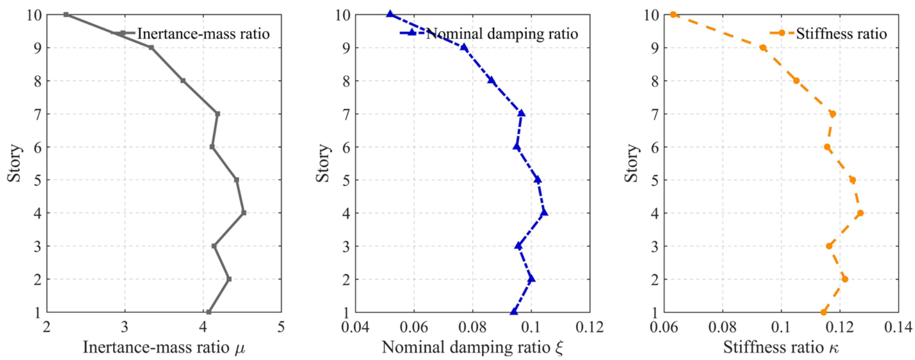

Fig. 16 Parameter distribution (M3)

Table 14 Damping deformation enhancement ratios α of inerter system

Floor number n	1	2	3	4	5	6	7	8	9	10
Proposed method	2.39	2.21	2.25	2.38	2.45	2.49	2.57	2.53	2.29	1.37
Fixed-point method (Ikago et al. 2012a, b, c)	1.89	1.91	1.94	1.97	1.99	2.00	1.99	1.96	1.90	1.84

effectively controlled when the inerter system is activated, and the performance of the controlled structure are almost the same. However, as the Table 13 shows, the damping forces of the inerter systems designed by the proposed are evidently reduced compared to that designed by the fixed-point method. The comparison of damping deformation enhancement ratios α of the two methods are listed in Table 14. It can be seen the deformation of the damping element inside the inerter system is enlarged based on the damping enhancement design principle.

5 Conclusions

This study proposed a demand-oriented design method for TVMDs incorporated into an MDOF structure ensuring its damping enhancement effect. Considering the inherent damping of the primary structure, the stochastic response of non-classically damped structure is obtained based on the random vibration theory. The design examples using three different types of benchmark structure exemplified the feasibility and efficiency of the proposed design method for practical use. The following conclusions are drawn:

(1) The target performance demand can be achieved with a smaller damping coefficient of the inerter system with the proposed design concept than that obtained by conventional method. That is, a high energy dissipation efficiency can be obtained by minimizing the nominal damping ratio of the inerter system because of the magnified damping enhancement. And the economic cost is also considered in this method.
(2) The proposed design method provides a topological damping enhancement approach for determining the parameter distribution pattern along the MDOF structure based on inter-story drifts; that is, the parameters for the inerter system are determined such that their distribution is positively correlated with that of the response amplitudes. The cost efficiency can be further increased by choosing an appropriate exponent that reflects the degree of positive correlation between the inerter system parameters and the response amplitudes.
(3) The utilization of the harmonic excitation method and complex modal analysis simplifies the calculation of the stochastic response of MDOF structures and makes it possible to take the inherent damping of the primary structures into account.
(4) All of the key parameters of the inerter system can be treated as design variables in the optimization method. Therefore, it is not necessary to specify an additional mass ratio before optimization, as in most existing methods.
(5) Although only one specific type of inerter system is considered in this study, the proposed parametric design method for MDOF structures is also expected to be applicable to other inerter systems with different mechanical layouts.

Acknowledgements The authors wish to acknowledge the National Natural Science Foundation of China, the Natural Science Foundation of Shandong Province, the Science and Technology Planning Project of Guangdong Province, and the Ministry of Science and Technology of the People´s Republic of China for finding this study. And the authors also appreciate Kohju Ikago of Tohoku University for his help in interpreting the significance of the results of this study.

Funding This study was funded by the National Natural Science Foundation of China (Grant No. 51978525), the Natural Science Foundation of Shandong Province (No. ZR2018BEE033), the Science and Technology Planning Project of Guangdong Province, China (No. 2018B02028003), and the National Key R&D Program of China (No. 2021YFE0112200).

Availability of data and material The datasets and materials of this research are available from corresponding author for rational request.

Declarations

Conflict of interest The authors declare that they have no conflict of interest.

References

Arakaki T, Kuroda H, Arima F, Inoue Y, Baba K (1999) Development of seismic devices applied to ball screw : Part 1 Basic performance test of RD-series. J Architect Build Sci 5(8):239–244 **(in Japanese)**

Asai T, Araki Y, Ikago K (2017a) Energy harvesting potential of tuned inertial mass electromagnetic transducers. Mech Syst Signal Proc 84:659–672. https://doi.org/10.1016/j.ymssp.2016.07.048

Asai T, Araki Y, Ikago K (2017b) Structural control with tuned inertial mass electromagnetic transducers. Struct Control Health Monit 25(2):e2059. https://doi.org/10.1002/stc.2059

China Ministry of Housing and Urban-Rural Construction (2015) Technical specification for steel structure of tall building (JGJ 99–2015). China Architecture & Building Press, Beijing, China

Chopra AK (2012) Dynamics of structures: theory and applications to earthquake engineering. Prentice Hall, New York

Den Hartog JP (1956) Mechanical vibrations. Dover, New York

Domenico DD, Qiao HS, Wang QH, Zhu ZW, Marano G (2020) Optimal design and seismic performance of Multi-Tuned Mass Damper Inerter (MTMDI) applied to adjacent high-rise buildings. Struct Design Tall Spec Build 29(14):e1781. https://doi.org/10.1002/tal.1781

Furuhashi T, Ishimaru S (2008) Mode control seismic design with dynamic mass. In: the 5th International Conference on Urban Earthquake Engineering.

Gonzalez BA, Clare LR, Neild SA, Burrow SG, Inman DJ (2015) An electromagnetic vibration absorber with harvesting and tuning capabilities. Struct Control Health Monit 22(11):1359–1372. https://doi.org/10.1002/stc.1748

Gonzalez-Buelga A, Clare LR, Neild SA, Jiang JZ, Inman DJ (2015) An electromagnetic inerter-based vibration suppression device. Smart Mater Struct 24(5):055015. https://doi.org/10.1088/0964-1726/24/5/055015

Hao LF, Zhang RF, Jin K (2017) Direct design method based on seismic capacity redundancy for structures with metal yielding dampers. Earthq Eng Struct Dyn. https://doi.org/10.1002/eqe.2977

Høgsberg J, Krenk S (2016) Calibration of piezoelectric RL shunts with explicit residual mode correction. J Sound Vib 386:65–81. https://doi.org/10.1016/j.jsv.2016.08.028

Housner GW, Bergman LA, Caughey TK, Chassiakos AG, Claus RO, Masri SF, Skelton RE, Soong TT, Spencer BF, Yao JTP (1997) Structural control: past, present, and future. J Eng Mech 123(9):897–971. https://doi.org/10.1061/(ASCE)0733-9399(1997)123:9(897)

Igusa T, Kiureghian AD (1985) Dynamic response of multiply supported secondary systems. J Eng Mech 111(1). https://doi.org/10.1061/(ASCE)0733-9399(1985)111:1(20)

Ikago K, Saito K, Inoue N (2012a) Seismic control of single-degree-of-freedom structure using tuned viscous mass damper. Earthq Eng Struct Dyn 41(3):453–474. https://doi.org/10.1002/eqe.1138

Ikago K, Saito K, Inoue N (2012b) Seismic control of single-degree-of-freedom structure using tuned viscous mass damper. Earthq Eng Struct D 41(3):453–474. https://doi.org/10.1002/eqe.1138(inEnglish)

Ikago K, Sugimura Y, Saito K, Inoue N (2012c) Modal response characteristics of a multiple-degree-of-freedom structure incorporated with tuned viscous mass dampers. J Asian Archit Build Eng 11(2):375–382. https://doi.org/10.3130/jaabe.11.375

Ikago K, Sugimura Y, Saito K, Inoue N (2014) Modal response characteristics of seismic controlled MDOF shear building using tuned viscous mass dampers. J Struct Constr Eng 79(697):367–374 **(in Japanese)**

Ikago K, Saito K, Sugimura Y, Inoue N (2010) Optimum seismic response control of multiple degree of freedom structures using tuned viscous mass dampers. In: Proceedings of the Tenth International Conference on Computational Structures Technology, Valencia, Spain.

Japan Society of Seismic Isolation (2007) Design and construction manual for passively controlled buildings. Tokyo, Japan

Kawamata S (1973) Development of a vibration control system of structures by means of mass pumps. University of Tokyo, Institute of Industrial Science

Kawamata S (1989) Liquid type mass damper with elongated discharge tube. Tokyo, Japan: Mitsubishi Jukogyo Kabushiki Kaisha.

Kida H, Ikago K, Inoue N (2012) Applicability of force-restricted tuned viscous mass dampers to high-rise buildings subjected to long-period ground motions. In: the 15th World Conference on Earthquake Engineering.

Kuroda H, Arima F, Baba K, Inoue Y (2000) Principles and characteristics of viscous damping devices (gyro-damper), the damping forces which are highly amplified by converting the axial movement to rotary one. In: the 12th World Conference on Earthquake Engineering.

Lazar IF, Neild SA, Wagg DJ (2014) Using an inerter-based device for structural vibration suppression. Earthq Eng Struct Dyn 43(8):1129–1147. https://doi.org/10.1002/eqe.2390

Li L, Hu YJ (2016) State-space method for viscoelastic systems involving general damping model. AIAA J 54(10). https://doi.org/10.2514/1.J054180

Lin JH, Zhang YH, Li QS, Williams FW (2004) Seismic spatial effects for long-span bridges, using the pseudo excitation method. Eng Struct 26(9):1207–1216. https://doi.org/10.1016/j.engstruct.2004.03.019

Makris N, Kampas G (2016) Seismic protection of structures with supplemental rotational inertia. J Eng Mech 142(11):04016089. https://doi.org/10.1061/(asce)em.1943-7889.0001152

Mathworks, (2017) MATLAB R2017b. Mathworks Inc, MA

McKenna F, Fenves G, Scott MH (2000) Open system for earthquake engineering simulation. University of California, Berkeley, CA, Pacific Earthquake Engineering Research Center

Nakaminami S, Ikago K, Inoue N, Kida H (2012) Response characteristics of a base-isolated structure incorporated with a force-restricted viscous mass damper. In: the 15th World Conference on Earthquake Engineering, Lisbon, Portugal.

Nakaminami S, Kida H, Ikago K, Inoue N (2017) Dynamic testing of a full-scale hydraulic inerter-damper for the seismic protection of civil structures. In: Proceedings of the 7th International Conference on Advances in Experimental Structural Engineering, Pavia Italy.

Nakamura Y, Fukukita A, Tamura K, Yamazaki I, Matsuoka T, Hiramoto K, Sunakoda K (2014) Seismic response control using electromagnetic inertial mass dampers. Earthq Eng Struct Dyn 43(4):507–527. https://doi.org/10.1002/eqe.2355

Nakamura Y, Watanabe H, Kawamata S (1988) Seismic response control of structures by accelerated liquid mass damper. In: Proceedings of the Ninth World Conference on Earthquake Engineering, Tokyo-Kyouto, Japan.

Nakamura Y, Hanzawa T, Isoda K (2017) Performance-based placement design of tuned inertial mass dampers. In: World Conference on Seismic Isolation, Energy Dissipation and Active Vibration Control of Structures.

Ogino M, Sumiyama T (2014) Structural design of a high-rise building using tuned viscous mass dampers installed across three consecutive storeys. In: Proceedings of the Twelfth International Conference on Computational Structures Technology, Stirlingshire, Scotland.

Ohtori Y, Christenson RE, Spencer BF, Dyke SJ (2004) Benchmark control problems for seismically excited nonlinear buildings. J Eng Mech 130(4):366–385. https://doi.org/10.1061/(ASCE)0733-9399(2004)130:4(366)

Pan C, Zhang RF, Luo H, Li C, Shen H (2018) Demand-based optimal design of oscillator with parallel-layout viscous inerter damper. Struct Control Health Monit 25(1):e2051. https://doi.org/10.1002/stc.2051

Pan C, Zhang RF (2018) Design of structure with inerter system based on stochastic response mitigation ratio. Struct Control Health Monit:e2169. https://doi.org/10.1002/stc.2169

Saeed TE, Nikolakopoulos G, Jonasson JE, Hedlund H (2015) A state-of-the-art review of structural control systems. J Vib Control 21(5):919–937. https://doi.org/10.1177/1077546313478294

Saito K, Kurita S, Inoue N (2007) Optimum response control of 1-DOF system using linear viscous damper with inertial mass and its Kelvin-type modeling. J Struct Constr Eng Architect I Jpn 53B:53–66 **(in Japanese)**
Saito K, Sugimura Y, Nakaminami S, Kida H, Inoue N (2008) Vibration tests of 1-story response control system using inertial mass and optimized softy spring and viscous element. In: the 14th World Conference on Earthquake Engineering.
Saitoh M (2012) On the performance of gyro-mass devices for displacement mitigation in base isolation systems. Struct Control Health Monit 19(2):246–259. https://doi.org/10.1002/stc.419
Soong TT, Spencer JBF (2002) Supplemental energy dissipation: state-of-the-art and state-of-the practice. Eng Struct 24(3):243–259. https://doi.org/10.1016/S0141-0296(01)00092-X
Spencer JBF, Nagarajaiah S (2003) State of the art of structural control. J Struct Eng 129(7):845–856. https://doi.org/10.1061/(ASCE)0733-9445(2003)129:7(845)
Sugimura Y, Goto W, Tanizawa H, Saito K, Nimomiya T (2012) Response control effect of steel building structure using tuned viscous mass damper. In: the 15th World Conference on Earthquake Engineering.
Swift SJ, Smith MC, Glover AR, Papageorgiou C, Gartner B, Houghton NE (2013) Design and modelling of a fluid inerter. Int J Control 86(11):2035–2051. https://doi.org/10.1080/00207179.2013.842263
Symans MD, Charney FA, Whittaker AS, Constantinou MC, Kircher CA, Johnson MW, McNamara RJ (2008) Energy dissipation systems for seismic applications: current practice and recent developments. J Struct Eng 134(1):3–21. https://doi.org/10.1061/(ASCE)0733-9445(2008)134:1(3)
Taflanidis AA, Giaralis A, Patsialis D (2019) Multi-objective optimal design of inerter-based vibration absorbers for earthquake protection of multi-storey building structures. J Franklin I. https://doi.org/10.1016/j.jfranklin.2019.02.022
Veletsos AS, Ventura CE (1986) Modal analysis of non-classically damped linear systems. Earthq Eng Struct Dyn 14:217–243. https://doi.org/10.1002/eqe.4290140205
Wang ZX, Giaralis A (2021) Enhanced motion control performance of the tuned mass damper inerter through primary structure shaping. Structural Des Tall Special Build 28(8):e2756. https://doi.org/10.1002/stc.2756
Wang FC, Hong MF, Lin TC (2011) Designing and testing a hydraulic inerter. Proc Inst Mech Eng Part C J Eng Mech Eng Sci 225(C1):66–72. https://doi.org/10.1243/09544062jmes2199
Xu YL, Zhang WS, Ko JM, Lin JH (1999) Pseudo-excitation method for vibration analysis of wind-excited structures. J Wind Eng Ind Aerodyn 83:443–454. https://doi.org/10.1016/S0167-6105(99)00092-6
Yang JN, Lei Y, Pan SW, Huang N (2003) System identification of linear structures based on Hilbert-Huang spectral analysis. Part 2: Complex modes. Earthq Eng Struct Dyn 32:1533–1554. https://doi.org/10.1002/eqe.288
Yao JTP (1972) Concept of structural control. J Struct Div 98(ST7):1567–1574
Zhang RF (2014) Seismic response analysis of base-isolated vertical tank. Tongji University, Shanghai
Zhang WS, Xu YL (1999) Dynamic characteristics and seismic response of adjacent buildings linked by discrete dampers. Earthq Eng Struct Dyn 28:1163–1185. https://doi.org/10.1002/(SICI)1096-9845(199910)28:10%3c1163::AID-EQE860%3e3.0.CO;2-0
Zhang RF, Zhao ZP, Pan C, Ikago K, Xue ST (2020) Damping enhancement principle of inerter system. Struct Control Health Monit:e2523. https://doi.org/10.1002/stc.2523

Authors and Affiliations

Ruifu Zhang[1,2] · Minjun Wu[1,2] · Chao Pan[3] · Chao Wang[1,2] · Linfei Hao[4]

[1] State Key Laboratory of Disaster Reduction in Civil Engineering, Tongji University, Shanghai 200092, China

[2] Department of Disaster Mitigation for Structures, Tongji University, Shanghai 200092, China

[3] College of Civil Engineering, Yantai University, Yantai 264005, China

[4] Earthquake Engineering Research & Test Center, Guangzhou University, Guangzhou 510405, China